nature food

ARTICLES

https://doi.org/10.1038/s43016-021-00432-4

Civil war hinders crop production and threatens food security in Syria

Xi-Ya Li[1,2], Xi Li[1]✉, Ziying Fan[3], Li Mi[4], Tarek Kandakji[5], Zhen Song[6], Deren Li[1] and Xiao-Peng Song[2]✉

Assessing the impact of violent conflict on Syrian agriculture is challenging given data limitations and attributability issues. Using satellite data at 30 m spatial resolution, we found that the extent of productive cropland showed greater interannual variability and spatial heterogeneity after the start of the civil war in 2011. Using changes in satellite-based night-time light as a proxy for war impact intensity, we also found that cropland close to severely impacted urban settlements faced greater disruption. Fixed-effects models revealed the relationship between productive cropland and precipitation for the pre-war period, whereas a counterfactual scenario constructed for the period 2012–2019 showed substantial variation at the regional level. While the ongoing conflict promoted cropland cultivation in safer zones, cropland reduction took place in the country's northwest and southeast regions. Our study demonstrated the combined utility of daytime and night-time satellite data to assess food insecurity in extreme environments and can help guide distribution of food and aid in Syria.

The long-lasting Syrian civil war, which began in March 2011, is considered the most severe humanitarian disaster of the 21st century to date. In addition to being responsible for a large number of dead, injured and refugees, the war has deteriorated basic living conditions for Syrian civilians. The World Food Programme reported that 9.3 million people in Syria suffered food shortages and 2.2 million people were at risk of food insecurity in 2020[1]. The food insecurity situation also escalated tensions between the Syrian central government and the Kurdish autonomous region, which stopped exporting wheat to government-controlled regions[2]. The war and the consequent collapse of the economy also constrained access to farming inputs and damaged supply-chain infrastructure, making Syrian agriculture much less productive; according to a recent report[3], Syria's wheat production in 2018 (1.2 Mt) was only 30% of the average level of the pre-war period (2002–2011). Although the Syrian government tried to import more food from the international market, it could not afford to meet the necessities of all Syrian civilians, contributing to a 20-fold increase in food prices in 2020 relative to pre-war levels[4].

Given the dangers of conducting field surveys in conflict zones, Earth observation satellites can provide a unique and direct data source for monitoring agricultural activities over an entire region. Satellite-based remote sensing has proved to be a critical technique in evaluating the socioeconomic and environmental impacts of wars in several countries, such as Sudan[5,6], Bosnia and Herzegovina[7], Democratic Republic of the Congo[8], Syria[9,10] and Yemen[11,12]. In these studies, night-time light (NTL) data and daytime satellite data were used to evaluate the destruction of human settlements and the loss of agricultural land as direct and/or indirect evidence of war conflicts. In Syria, specifically, research involving remote sensing has been carried out to evaluate the impact of war on agriculture; one analysis based on vegetation indices suggested that irrigated agricultural production had dropped by more than 15% in Syria's Orontes basin during 2000–2013—and the conflict was shown to be a major cause in addition to drought[12]. It is known that the emergence of the Islamic State of Iraq and al Shams (ISIS) has significantly altered the progress of the war, and thus scholars became interested in monitoring agricultural activities in ISIS-controlled zones[13,14]. Combining the Moderate Resolution Imaging Spectroradiometer (MODIS) vegetation index and agricultural statistical data, it was estimated that barley and wheat production in ISIS-controlled Syrian and Iraqi territory was sustained during 2014–2015 despite the impact of the conflict because ISIS used agricultural exports to gain income[13]. Another study, using MODIS-estimated cultivated land extent and farming intensity, revealed that ISIS-controlled territory in Syria and Iraq experienced an expansion of cultivated cropland along with conversion of cultivated land to fallow, suggesting that ISIS had reshaped agriculture in its territory[14].

Although these studies have suggested that the Syrian civil war has indeed impacted crop cultivation and domestic food production, most studies focused on a limited part of Syria over a short time period (such as ISIS-controlled territory after the war broke out[13,14]). The primary challenge in quantitatively evaluating the long-term impact of the war over a larger area is to separate the confounding factor of precipitation, which has significantly affected Syrian agriculture in both the pre-war period[15] and during the war[14]. Syria experienced severe droughts in 1998–2000, 2007–2009 and 2014[13]. The 2007–2009 drought, which was linked to climate change[16,17], was considered one of the driving factors of the 2011 unrest[18].

In this study we evaluated the impact of the Syrian civil war on the country's productive cropland dynamics from 1998 to 2019. We used time series of Landsat images and MODIS data to map the annual extent of productive cropland at 30 m resolution over the study period. Our productive cropland map represented the fields that showed a complete growth cycle as well as sufficient greenness in the spectral feature space, and thus represented the actively

[1]State Key Laboratory of Information Engineering in Surveying, Mapping and Remote Sensing, Wuhan University, Wuhan, China. [2]Department of Geosciences, Texas Tech University, Lubbock, TX, USA. [3]School of Public Economics and Administration, Shanghai University of Finance and Economics, Shanghai, China. [4]Environmental Computational Science and Earth Observation Laboratory, Ecole Polytechnique Fédérale de Lausanne, Sion, Switzerland. [5]Yale Center for Earth Observation, Yale School of the Environment, Yale University, New Haven, CT, USA. [6]Department of Geographical Sciences, University of Maryland, College Park, MD, USA. ✉e-mail: lixi@whu.edu.cn; xiaopeng.song@ttu.edu

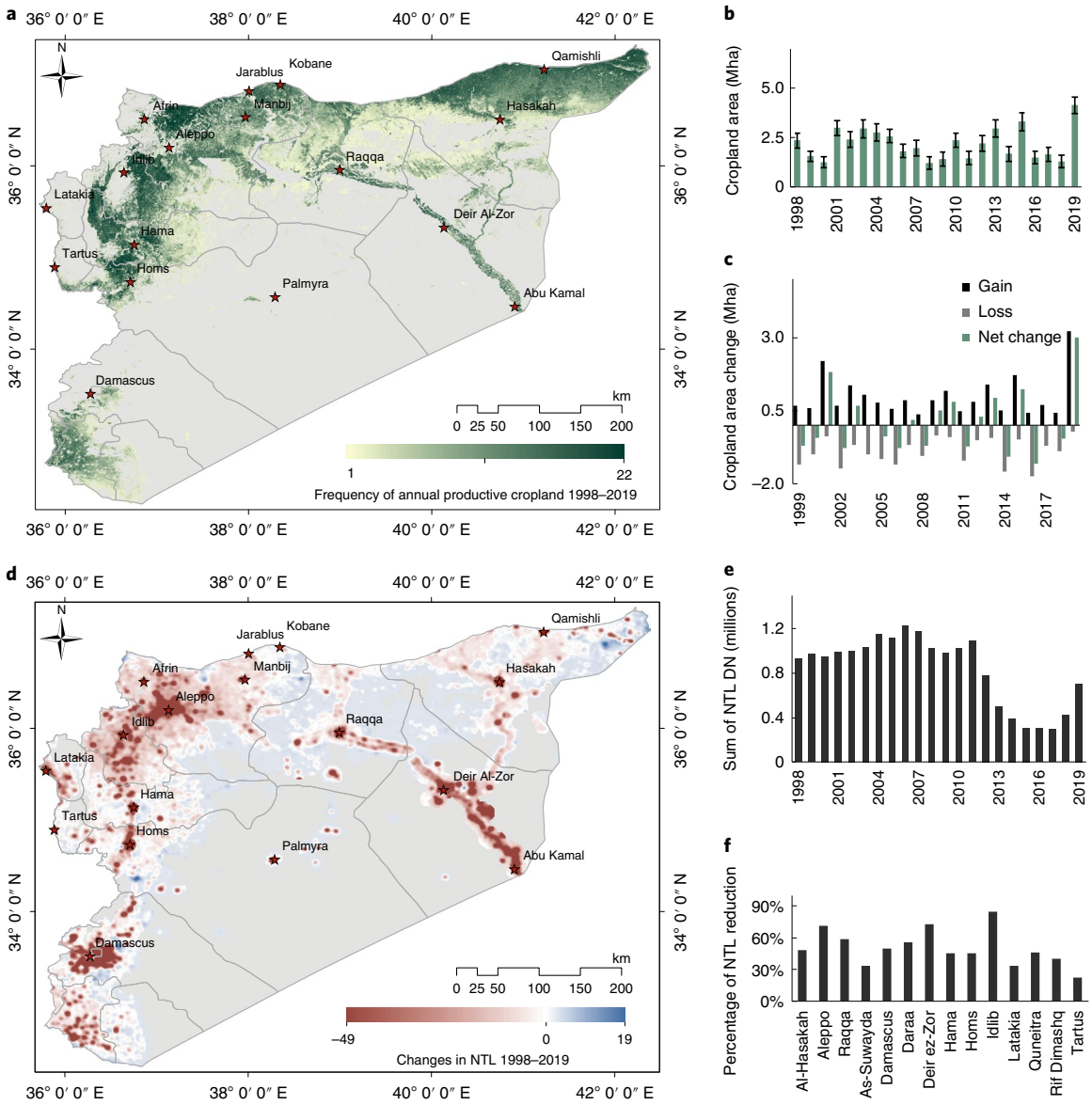

Fig. 1 | Productive cropland and NTL dynamics in Syria. a, Frequency of productive cropland, defined as the number of years a pixel is mapped as productive cropland between 1998 and 2019. **b**, Annual productive cropland area in Syria. Error bars represent 95% confidence intervals derived from sample-based classification accuracy estimates. **c**, Annual cropland change compared with the previous year. **d**, Average NTL intensity change between 1998–2011 and 2012–2019. **e**, Time series of total NTL digital numbers (DN) in Syria. **f**, Percentage of NTL reduction during the war for each governorate. Damascus in panel **f** refers to the municipalities of the Damascus governorate.

cultivated lands with harvestable production. We used changes in satellite-derived NTL as a proxy to represent the war intensity over the country, especially urban settlements. To evaluate the spatial heterogeneity of the war impact, we investigated changes in productive cropland area as a function of distance to the nearest major conflict zones. We then conducted spatially explicit panel regression analysis to quantify the contributions of precipitation and war conflicts to cropland changes. We constructed a fixed-effects model between annual cropland area and annual precipitation for 1998–2011 (that, is the pre-war period), and predicted annual cropland area using annual precipitation for 2012–2019 (that is, wartime) as the non-war counterfactual scenario. By comparing the counterfactual predictions with satellite-observed cropland for 2012–2019, we were able to isolate the impact of war and visualize its regional variations. This analysis allowed us to assess food security as affected by both natural and human disasters.

Results and discussion

Productive cropland dynamics in Syria. Based on satellite observations, Syria had 6.15 Mha of land area that were used as cropland from 1998 to 2019 (that is, the maximum extent across 22 yr), which covered 33% of Syria's total land area. Productive cropland in Syria was mainly distributed in the northeast and northwest parts of the country, in addition to the relatively stable cultivation along the Euphrates River (Fig. 1a). The three governorates with the largest 22 yr average cropland area were Al-Hasakah (0.70 Mha), Aleppo (0.59 Mha) and Hama (0.24 Mha) (Fig. 2). Croplands were also observed in the Raqqa and Deir ez-Zor governorates along the Euphrates River, while a large part of central–south Syria is covered by desert. The average coverage of productive croplands in the Rif Dimashq (southern Syria) and Homs (central Syria) governorates were only 2% and 3%, respectively. In the Homs governorate, cropland cultivation was mainly distributed in the northwest and central

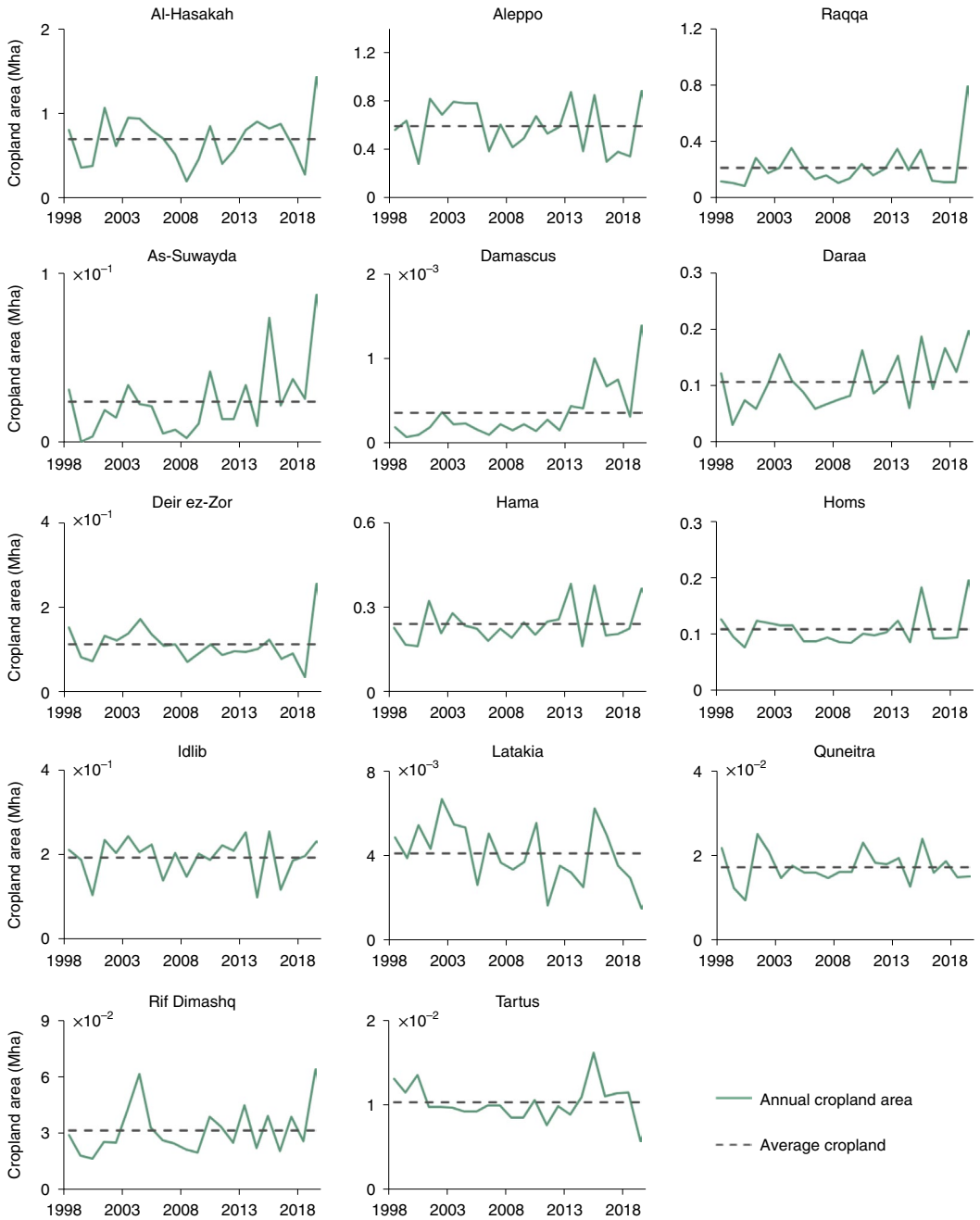

Fig. 2 | Annual productive cropland area for each governorate in Syria between 1998 and 2019. Damascus refers to the municipalities of the Damascus governorate. Areas were derived from annual classification maps without sample-based adjustment.

regions, and cropland around the oasis city of Palmyra was a major part of agriculture in the central region.

The annual cropland area in Syria ranged from 1.21 ± 0.31 Mha in 2000 to 4.15 ± 0.42 Mha in 2019 (Fig. 1b), with an average value of 2.17 Mha. During the two severe droughts experienced by the country (1998–2000 and 2007–2009), we observed a decrease in the productive cropland area, followed by an immediate recovery. The average cropland area was 1.70 Mha in 1998–2000 and 1.53 Mha in 2007–2009. Compared to the average cropland area of the entire 22 yr period, the average cropland area during the two drought events was 21% and 30% lower, respectively. During the 2007–2009 drought, the year 2008 witnessed the most noticeable reduction in productive cropland area (Fig. 1b). Consequently, some major agricultural governorates, such as Al-Hasakah, were affected by the drought event (Fig. 2). The average cropland area from 2007 to 2009 in Al-Hasakah was only 0.39 Mha, which was 43% lower than its long-term average (0.70 Mha), and the cropland area in 2008 was the lowest observed in the 22 yr period (0.21 Mha).

Since the start of the war in 2011, productive cropland dynamics showed greater interannual variability and spatial heterogeneity. In general, the net change in the annual cropland area appears to be more drastic than in the pre-war era (Fig. 1c). Both the largest annual cropland loss (in 2016) and gain (in 2019) occurred after 2011. Furthermore, the dynamics of cultivation areas between some governorates and their surrounding governorates became different (Supplementary Fig. 1). For instance, the two major agricultural governorates, Aleppo and Al-Hasakah, contained nearly equal

Table 1 | Regression coefficients for the attribution of productive cropland area and change

	Dependent variable		
	Productive cropland area (ha)		Productive cropland area change (ha)
Independent variables	1998–2019	1998–2011	2012–2019
Individual fixed effects	Yes	Yes	Yes
Time fixed effects	Yes	No	Yes
Precipitation × time_dummy	−0.014440*** (0.000204)		
Precipitation × distance × time_dummy	0.000934*** (7.93×10^{-6})		
Precipitation × distance	0.000394*** (6.82×10^{-6})	0.000541*** (7.86×10^{-6})	
Precipitation	0.036607*** (0.000217)	0.044048*** (0.000213)	
Distance × time_dummy	−0.184966*** (0.002178)		
Precipitation change			27.84671*** (2.950176)
NTL intensity change			0.490746** (0.160749)
Intercept	5.707769*** (0.054419)	0.414786*** (0.039150)	3042.610*** (351.5602)
Observations	2,881,538	1,833,706	1,584
R^2	0.746	0.752	0.504
Model name	All-period Model	Counterfactual Model	Wartime Model

Standard errors are shown in parentheses. **$P < 0.01$; ***$P < 0.001$.

cropland area from 2009 to 2012, but Aleppo's cropland area was evidently lower than Al-Hasakah's from 2012 to 2019.

Attribution of productive cropland area change. Before the war, changes in Syria's productive cropland area were mainly caused by variations in the arid and semi-arid climate where it was strongly dependent on precipitation[19]. For example, at the 25 km grid scale—which was equal to the resampled resolution of the precipitation data—precipitation could explain 84% of the variations in annual productive cropland area from 1998 to 2011 ($P < 0.001$, see Supplementary Information for details). The annual rainfall differed considerably between years, which exerted an influence on the annual productive cropland dynamics[20]. In general, favourable precipitation would promote the development of crops and increase the productive area of a season.

The drivers of cropland dynamics during wartime were quantified by panel regression analysis (Table 1, Wartime Model). Changes in productive cropland area during wartime positively correlated with both precipitation and the NTL change. Note that the change values were calculated by subtracting the average value of the pre-war period (that is, 1998–2011) from the annual observations during the war. The results indicated that changes in precipitation and NTL were responsible for 32% and 19% (estimated by the standardized regression coefficient[21]) of productive cropland area change during the war, respectively. Analysis at the 25 km grid scale showed that a one-unit decrease in NTL intensity would lead to about a 0.49 ha reduction in productive cropland area, and the average NTL change during the war led to a total reduction of about 0.19 Mha of productive cropland per year.

Additionally, according to the spatial pattern of wartime cropland change on the 25 km grid scale, we found that not only did the spatial grids with severe NTL reduction tend to have cropland reduction during the war, but cropland in the surrounding regions also decreased. Specifically, croplands located closer to the nearest urban settlements with severe NTL reduction faced a greater risk of reduction (Fig. 3). In the temporal domain, the value of the annual correlation coefficient (Fig. 3) suggested that the impact of the war slowly appeared a few years later after the war broke out, mainly since 2014 ($R^2 = 0.07$, $P < 0.001$). This progression might be attributed to the fact that the refugee crisis and the death toll caused by the war became more serious after 2013[22,23]. Moreover, the correlation between the distance to the nearest urban settlements with severe NTL reduction and changes in cropland area appeared to have weakened after 2018. This might be explained by two reasons. First, the war intensity was mitigated, shown as a lower death toll and a slower increase in refugee numbers compared to the early years of the war[22,23]. Second, the NTL data could be mainly reflecting the dynamics of the war impact intensity in the early years because NTLs tend to stabilize after being reduced to a very low level, even if the war continued.

Further evidence of how the war affected cropland dynamics was revealed from the All-period Model at the 1 km grid scale (Table 1, see Methods for details). The All-period Model includes a time dummy, which allowed us to simulate the outbreak of war and identify the impact of war by analysing the coefficients of the variables. Our modelling results indicated that the overall impact of precipitation on productive cropland area was reduced by 39% after the war broke out. Moreover, the heterogeneous effects of precipitation increased by 2.4 times, shown as the increased difference of precipitation impact among regions. The impact of precipitation was smaller within the vicinity of urban areas with severe NTL reduction. Based on the average precipitation value during the war, rural areas within a 53 km buffer around the urban areas with severe NTL reduction were considered to be affected by war in terms of cropland cultivation (see Supplementary Information for details).

Spatial heterogeneity of war impact on cropland cultivation. To better visualize the spatial heterogeneity of the impact of war on cropland cultivation, we modelled the relationship between annual cropland area and precipitation for the pre-war period at a 1 km grid scale (Table 1, Counterfactual Model), and then used this relationship to create a counterfactual scenario under the no-conflict assumption from 2012 to 2019. Assuming precipitation and war were the only determining factors, the differences between the predicted counterfactual scenario and satellite observations would represent the impact of war. The average differences in productive cropland area between satellite observations and the counterfactual scenario during the war are shown in Fig. 4. Negative values represent spatial grids where the observed cropland area is less than that predicted by the model using precipitation alone. These are

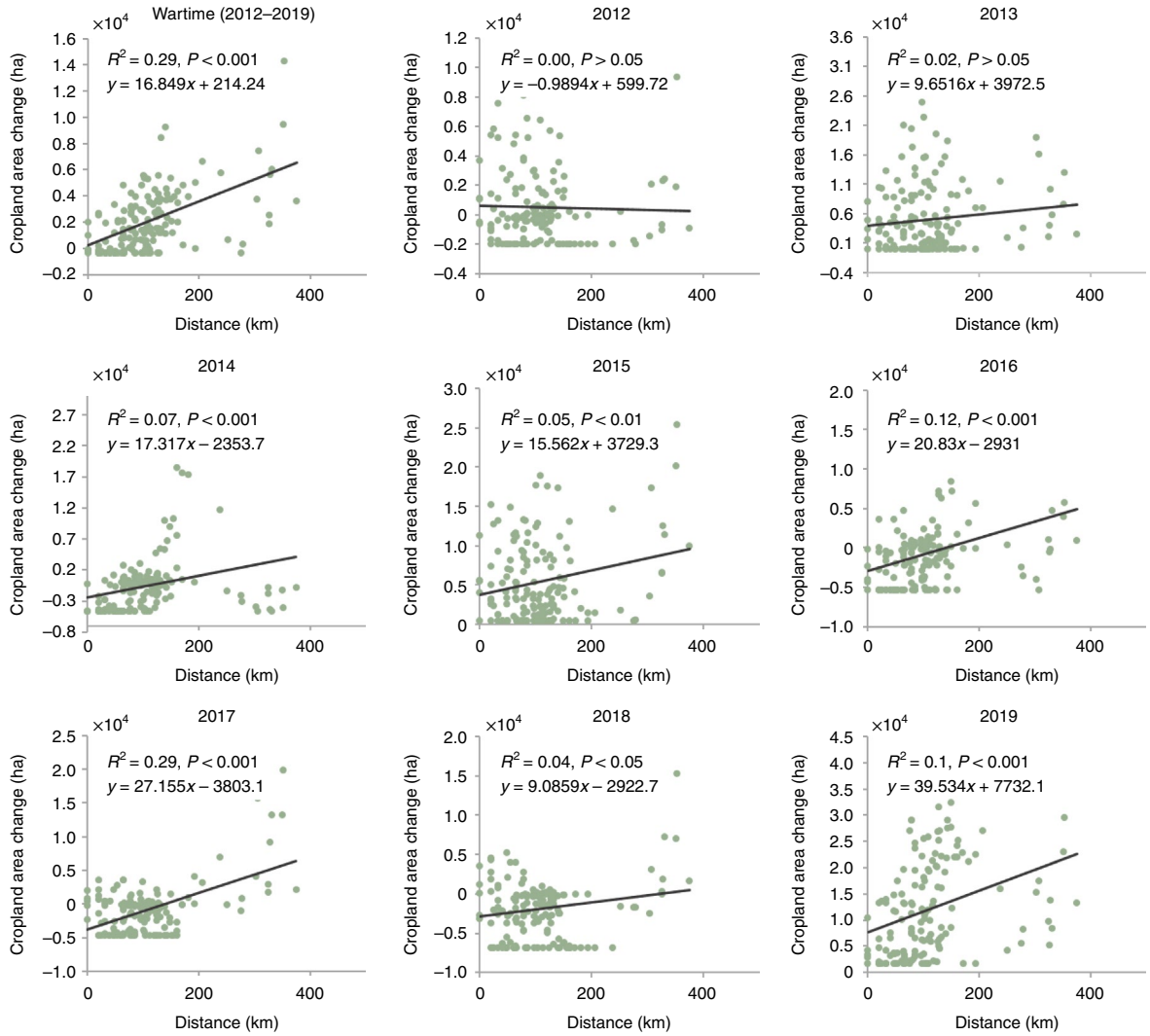

Fig. 3 | Relationship between changes in productive cropland area and the distance to the nearest urban settlements with severe NTL reduction. Severe NTL reduction was considered on a 25 km grid scale (n = 155). For the definition of the nearest urban area with severe NTL reduction, refer to the Supplementary Information. In the first subplot (row 1, column 1), cropland area change was calculated by subtracting the average cropland area before the war (1998–2011) from the average cropland area during the war (2012–2019). In the remaining subplots, cropland area change was calculated by subtracting the average cropland area before the war from the observed cropland area in a specific year. Note that outliers were handled by winsorizing with the threshold of 5%.

rural areas where the Syrian civil war has reduced cropland cultivation. Conversely, positive values represent spatial grids where the observed cropland area is more than the model predicted. These are rural areas where the war has promoted cropland cultivation. We note that the impact of irrigation was not explicitly investigated in this study, but the effect of irrigation might have been partially captured in the impact of war because irrigation infrastructure could be affected as a direct result of the war, which in turn affects crop production[24]. The findings presented in this study would benefit from future research by exploring irrigation mapping from satellite or other data sources, and quantifying the influence of irrigation on cropland change (see Supplementary Discussion for more details).

We observed in Fig. 4 extensive underpredicted spatial grids, which contributed to the increase in average cropland area during the war when the average rainfall was about 5% lower than the average before the war. We attributed the increase in cropland area during the war to two main factors. First, bare soil/fallow was converted to cropland (Supplementary Fig. 2, row B) because the war forced people to migrate to safer zones[23,25]. The steady increase in food demand in these safe zones, the need to achieve wheat self-sufficiency[26] and the taxes imposed on agricultural products[13] emphasized the role of agricultural development and encouraged people to reclaim land[14]. In addition to the direct demand in safer zones, the food demand in regions affected by the war might be spilled over, which encouraged crop cultivation in the relatively stable regions. For example, we observed extensive underpredicted spatial grids in the northern Al-Hasakah governorate which served as a large, relatively stable breadbasket, and was under Kurdish control after the war broke out[27]. Consistent with our results, Eklund et al.[14] and Mohamed et al.[28] also reported that a certain area of bare soil/fallow was converted to cropland in the northern Al-Hasakah governorate during the war. Second, cash crops were converted to food crops because more people were in need for basic food and livelihood support[29]. This type of land-use conversion was evident in Damascus, the capital of Syria (Fig. 4). Before Damascus achieved stability and came under the control of the Syrian Government Army, the eastern part of Damascus was besieged, forcing people to grow crops to survive[24,30]. In addition, the war restricted the food

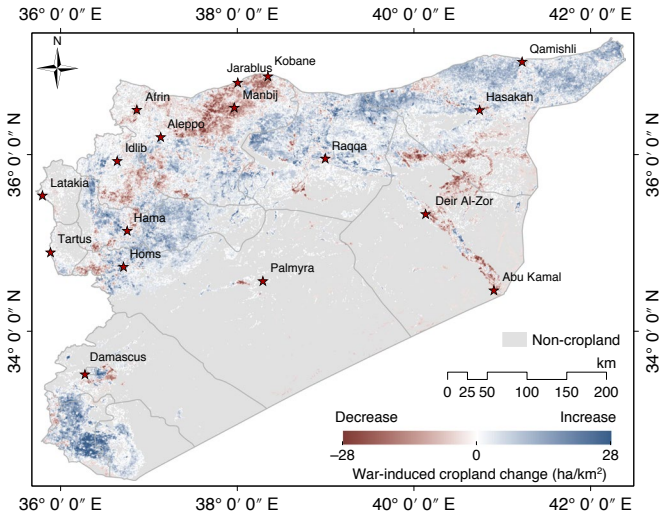

Fig. 4 | Spatial heterogeneity of the impact of war on agricultural cultivation in Syria. Spatial heterogeneity was derived as the average difference between satellite observations and counterfactual predictions from a fixed-effects model during 2012 to 2019 on a 1 km grid scale. The fixed-effects model was calibrated using precipitation during the pre-war period as the driving factor of cropland change. Negative values (red) represent spatial grids where satellite-observed cropland area is less than predicted by the model, indicating the war has reduced cropland cultivation. Positive values (blue) represent spatial grids where satellite-observed cropland area is higher than predicted by the model, indicating the war has promoted cropland cultivation.

trade, disrupted supply chains and might have made it difficult for the Syrian government to obtain wheat[2,31]. Satellite images revealed that a number of land patches with fruit trees were converted to cropland during the war in the Damascus governorate (Supplementary Fig. 2, row A)—fruits were a luxury that had been replaced by necessities[32].

The results presented in Fig. 4 show that overpredicted grids were spatially more clustered than the underpredicted grids. The overpredicted grids were mainly distributed in the northwest and southeast of Syria. In the northwest, the overpredicted grids were mainly located in the Aleppo and Idlib governorates. In the southeast, most of the overpredicted grids were distributed in the Deir Al-Zor governorate and the southern Al-Hasakah governorate. Our analysis also revealed some scattered patches of overpredicted grids, such as the rural areas near the city of Hama, the exterior of the Damascus governorate and the west of Palmyra city (Supplementary Fig. 2, row C), which was severely damaged by ISIS in 2015[33]. These areas with overpredicted grids were probably subject to frequent military activity, resulting in the cropland there being poorly managed. Similarly, we observed overpredicted grids in rural areas located around Aleppo, which were invaded by multiple forces and thus suffered the most severe damage during the war. Since 2016, Aleppo has been divided between the Syrian government, ISIS, Kurdish forces and rebel groups[27]. Armed conflicts were inevitable between these forces, which resulted in about 200,000 civilians displaced and escaped[34], significant destruction of the irrigation canals[24], increased seed prices and disruption of the agriculture market[35]. Another reason that led to decreased cropland in some regions was that different armed groups prevented farmers from accessing their lands as a military strategy to weaken food supply in a besieged area controlled by an adversary[24,36]. The overpredicted grids in Deir ez-Zor and Al-Hasakah might be attributed to ISIS control of the area between 2014 and 2017[27]. The situation was extremely precarious in the ISIS-controlled zone, as it experienced numerous airstrikes and ground attacks from many forces, including the US army, Russian army, Syrian government forces and Kurdish forces[37]. Moreover, many farmers in the ISIS zones stated they had not sowed sufficient crops due to the lack of fertilizers, fuel and effective policies to guarantee the sale of agricultural products[38]. These findings highlight the potential interactions between violent conflicts, regime stability, human displacement, agriculture management and land cover change for a region in conflict.

Conclusions

The goal of our study was to analyse by means of satellite observations how the Syrian civil war had affected productive cropland. We found that productive cropland dynamics in Syria exhibited greater interannual variability and spatial heterogeneity during the period of war. Through a panel regression analysis and a subsequent counterfactual analysis that isolated the impact of precipitation, we revealed regional gains and losses in the productive cropland area that were attributable to the civil war. While the war has promoted agricultural development in certain regions, multiple clustered regions suffered from cropland loss and the inevitable food shortages. The resulting map of the impact of war (Fig. 4) provides a reference for scientists to further investigate the local effects of the war and may also guide international agencies such as the United Nations High Commissioner for Refugees in providing relief to impacted regions.

Methods

Data. *Satellite data.* We used Landsat data to map annual productive cropland extent from 1998 to 2019 because the free and open Landsat archive represents one of the best data sources for long-term land-cover and land-use analysis at a medium spatial resolution[39]. The Landsat Surface Reflectance images were provided by the US Geological Survey at a 16 day revisit cycle[40,41]. The dataset has been geometrically corrected to Level-1TP (L1TP), atmospherically corrected using the Landsat Ecosystem Disturbance Adaptive Processing System (LEDAPS) and the Land Surface Reflectance Code (LaSRC)[42,43] and includes a cloud, shadow, water and snow mask[44]. We used all the Landsat 5, 7 and 8 images from 1998 to 2019 and processed the data on Google Earth Engine[45]. In addition, we also acquired the Normalized Difference Vegetation Index (NDVI) from the Moderate Resolution Imaging Spectroradiometer (MODIS) Vegetation Indices Version 6[46] data as supplementary data for training and validation. This MODIS NDVI dataset (MOD13Q1) has been generated every 16 days at 250 m spatial resolution since 2000 and is widely used in mapping cropland and monitoring crop growth[47].

We used NTL satellite data as a proxy for analysing the impact of war[9,10]. Specifically, we used two data sources to produce the continuous time series of NTL from 1998 to 2019. The first data source is the annual composites of Defense Meteorological Satellites Program/Operational Linescan System (DMSP/OLS) images, which measured the global NTLs from 1992 to 2013 with a spatial resolution of 30 arcseconds. The second data source is the monthly composites of the Visible Infrared Imaging Radiometer Suite onboard the Suomi National Polar-Orbiting Partnership (S-NPP/VIIRS) images, which have measured the global NTLs from 2012 to present and have a spatial resolution of 15 arcseconds. In addition to the difference in spatial resolution, the S-NPP/VIIRS records NTL data with better radiometric quality than DMSP/OLS[48]. The two data sources were downloaded from Yale University (https://urbanization.yale.edu/data) and Colorado School of Mines (https://eogdata.mines.edu/download_dnb_composites.html), respectively. The details of processing the two datasets, including intercalibration between them and removal of gas flares, are described in Supplementary Methods.

Climate data. We used the Precipitation Estimation from Remotely Sensed Information using Artificial Neural Networks–Climate Data Record (PERSIANN-CDR) dataset developed by the Center for Hydrometeorology and Remote Sensing at the University of California[49]. The precipitation dataset has a spatial resolution of 0.25°. In this study we resampled the dataset to 0.225° × 0.225° (about 25 km grid resolution) in World Geodetic System 1984 (WGS84) and calculated the annual total precipitation by summing precipitation in the wet season (November–April).

Administrative boundary. The administrative boundary data were collected from version 2.8 of the GADM database of Global Administrative Areas (https://gadm.org/download_country_v2.html). Note that the study area does not include Golan Heights.

Land cover classification. According to the major crop types and crop calendar in Syria, we defined the vegetation growing window from December to May (see Supplementary Information for details). We collected 13,970 Landsat images in total including 4,262, 6,750 and 2,958 from Landsat 5 Thematic Mapper (TM), Landsat 7 Enhanced Thematic Mapper Plus (ETM+) and Landsat 8 Operational Land Imager (OLI) and Thermal Infrared Sensor (TIRS), respectively. Seven spectral bands including blue, green, red, near-infrared and shortwave infrared reflectance, and brightness temperature, and the calculated Normalized Difference Vegetation Index (NDVI)[50] and Normalized Difference Water Index (NDWI)[51] were used in the cropland mapping. We derived a series of statistical metrics from the Landsat data for both growing and non-growing seasons for each year from 1998 to 2019. For each year, there were 90 metrics in total, including: (1) reflectance values that represented the selected percentiles (15th, 25th, 50th, 75th and 85th percentiles); and (2) NDVI and NDWI values that represented the selected percentiles (15th, 25th, 50th, 75th and 90th percentiles), of both growing and non-growing seasons.

We used a supervised classification approach to map annual productive cropland in Syria. We collected training data manually by visual interpretation using growing-season and non-growing-season Landsat images, time series of NDVI from Landsat and MODIS, and high-resolution images on Google Earth. In the process of selecting training samples, we considered two critical factors to ensure the representativeness and accuracy of the training: (1) the training samples need to be selected from multiple years, covering the dry year (2007), the wet year (2002) and the year with moderate precipitation (2012) to ensure the diversity of the samples; (2) high-resolution images on Google Earth are adequate to ensure the accuracy of visual interpretation of various land-cover types. In the end, 238,471 training pixels covering the years 2002, 2007, 2012, 2017, 2018 and 2019 were selected on the Google Earth Engine platform.

We chose random forests (RF) as the classification algorithm as its effectiveness has been demonstrated in land-cover classification[52,53]. The RF classifier was trained on the High Performance Computing Center (HPCC) clusters at Texas Tech University. The input features of the RF model were the annual Landsat metrics and elevation data from the Shuttle Radar Topography Mission (SRTM) digital elevation model (DEM)[54], which was included to eliminate the terrain factors that could confuse the spectral characteristics of certain land-cover types[55]. The trained RF model was applied to create the annual cropland classification maps from 1998 to 2019.

We designed a stratified random sample and computed accuracy metrics for the annual cropland maps following the good-practice guide[56]. We also used the validation sample to adjust the map-based annual cropland area estimates and derived 95% confidence intervals as reported in Fig. 1b (see Supplementary Methods for details).

Extraction of NTL reduction area. NTL provides an opportunity to detect electricity supply, which represents economic activity[57]. Since the Syrian war broke out, there have been intensive conflicts spreading over the country. The conflicts have impacted the social-economy, destroyed cities, damaged the power infrastructure and resulted in massive migration and death, which lead to a reduction in NTL. Results of previous research had shown that reduction in NTL in a region undergoing conflict generally represented the intensity of conflict in that region[9,58,59]. Based on this hypothesis, Levin has confirmed that NTL can serve as a potential metric to track global and regional conflict zones[59]. In this article the extracted urban area with severe NTL reduction was assumed to be the major zone impacted by the conflict, which was cross-inspected with multi-source data, including news reports, the area controlled by each regime from the Syria Live Map[27], geospatial death data from the Uppsala Conflict Data Program (Supplementary Fig. 3)[60] and the damage assessment of cities from the United Nations Office for the Coordination of Humanitarian Affairs[61]. Details about extracting urban areas with severe NTL reduction are described in the Supplementary Methods. Cross-checking results demonstrated that the areas where NTL is severely reduced, such as near the cities of Aleppo, Idlib and Deir ez-Zor, are almost all battlefields or around major conflict zones. Therefore, we adopted NTL reduction as a measure of the war impact intensity in urban settlements and assessed the location of the major conflict zones.

Cropland change attribution. The cropland dynamics could be attributed to natural and non-natural factors during the war. Many natural factors (for example, precipitation, evapotranspiration and temperature) can exert an influence on productive cropland area, where precipitation is of high variability and can be directly measured[19,28,62,63]. Most of the non-natural factors were affected by the war directly or indirectly (for example, through labour displacement, irrigation infrastructure, agriculture market or regime policy changes). Based on our analysis and evidence from various relevant studies[12,14,64], we primarily attributed the cropland dynamics during the war to the impacts of precipitation and conflict.

We designed four models to analyse the attribution of cropland dynamics on different spatial and temporal scales (a summary of the model details is given in Supplementary Table 1). First, before the war, the cropland dynamics were mostly attributable to precipitation[19,28,62]. Therefore, we constructed the Pre-war Model to investigate the relationship between precipitation and productive cropland area. Second, we designed the Wartime Model to investigate the attributions of the wartime cropland dynamics. The Wartime Model partly explained the wartime cropland dynamics by the variation of precipitation and the intensity of war (as measured by NTL reduction). Third, to evaluate the spatial heterogeneity of the impact of war and to further reveal how the war affected cropland dynamics, we constructed the All-period Model at a finer spatial resolution, which evaluated productive cropland area as a function of distance to the nearest urban area with severe NTL reduction. Finally, we constructed the Counterfactual Model to highlight the spatial details of the impact of war on productive cropland change during the war. The relationship between productive cropland area and precipitation was modelled for 1998–2011. Then we used the characterized relationship to predict annual productive cropland area using precipitation as input for 2012–2019, as the non-war counterfactual scenario. By comparing the counterfactual predictions with satellite-observed cropland area at 1 km resolution, we were able to visualize the heterogeneous impacts of war.

Pre-war Model. We estimated the pre-war relationship between annual precipitation and cultivated cropland area on the national, governorate, 25 km grid (0.225° × 0.225° in WGS84) and 1 km grid scales (0.008° × 0.008° in WGS84), respectively. The data preparation is described in the Supplementary Methods. For the national and governorate scales, the relationship was estimated by the following linear model:

$$C_t = \beta P_t + \lambda + \mu_t \quad (1)$$

where C_t and P_t represent the observed productive cropland area and precipitation in Syria (or individual governorate) in year t, respectively. λ is a constant term, μ_t denotes the error term and β is a coefficient that needs to be estimated. The equation reflects the impact of precipitation on the productive cropland area.

For the 25 km and 1 km grids, the relationship was estimated by the following two-way fixed-effects model, which allowed us to consider omitted variables:

$$C_{i,t} = \beta P_{i,t} + \lambda_i + \gamma_t + \mu_{i,t} \quad (2)$$

where $C_{i,t}$ and $_{Pi,t}$ represent productive cropland area and precipitation in grid i in year t, respectively. λ_i is an individual fixed effect that changes with grid i. γ_t is the time fixed effect, which varies with year t. $\mu_{i,t}$ denotes the error term. β is a coefficient that needs to be estimated.

Wartime Model. Then, we calculated the relationship between NTL change, precipitation change and productive cropland area change with a two-way fixed-effects model on the 25 km grid scale:

$$C\prime_{i,t} = \beta_1 P\prime_{i,t} + \beta_2 N\prime_{i,t} + \lambda_i + \gamma_t + \mu_{i,t} \quad (3)$$

where $C\prime_{i,t}$, $N\prime_{i,t}$ and $P\prime_{i,t}$ represent cropland area change, NTL intensity change and precipitation change in grid i in year t, respectively. λ_i is an individual fixed effect. γ_t is a time fixed effect. $\mu_{i,t}$ denotes the error term. β_1 and β_2 are coefficients that need to be estimated. β_1 represents the impact of precipitation change on the cropland area change, and β_2 represents the impact of NTL change on the cropland area change. In this analysis, the change values referred to the difference between wartime observations in a year and the average value of the pre-war period (that is, 1998–2011), which were calculated by subtracting the pre-war average from the annual observations during the war.

All-period Model. To evaluate the spatial heterogeneity of the impact of war and to further reveal how the war influenced cropland dynamics, we adopted equation (4) to estimate the effects of war, location, precipitation and their interaction on productive croplands. This analysis was implemented on the 1 km grid scale:

$$C_{i,t} = \beta_1 P_{i,t} + \beta_2 P_{i,t} D_i + \beta_3 P_{i,t} W_t + \beta_4 D_i W_t + \beta_5 P_{i,t} D_i W_t + \lambda_i + \gamma_t + \mu_{i,t} \quad (4)$$

where the dependent variable $C_{i,t}$ is the productive cropland area in grid i in year t, and $P_{i,t}$ is the precipitation. D_i is the Euclidean distance from grid i to the nearest urban area with severe NTL reduction. W_t is a dummy variable of war, which is 0 from 1998 to 2011, and 1 from 2012 to 2019. λ_i is an individual fixed effect. γ_t is a time fixed effect. $\mu_{i,t}$ denotes the error term. β_1, β_2, β_3, β_4, β_5 are coefficients that need to be estimated. β_1 represents the impact of precipitation on the cropland area. β_2 denotes how the impact of precipitation varied with D_i, indicating the spatial heterogeneity of precipitation impacts. β_3 represents the correction factor of the impact of precipitation on the cropland area during the war. β_4 represents the impact of the distance from grid i to the nearest urban area with severe NTL reduction during the war. β_5, the key parameter to be estimated in this article, captures the regional heterogeneous effects of precipitation on agriculture during wartime.

Counterfactual Model. The following analysis was designed to calibrate the cropland area during the war using the pre-war data and model (that is, 1998–2011), which used observed cropland area, precipitation and precipitation × distance as input (equation (5)). Note that precipitation × distance in this model was expected to exclude the interaction between precipitation

and distance. Then we applied the calibrated model to the war period (that is, 2012–2019) to predict the productive cropland area using observed precipitation and precipitation × distance as input. This analysis was implemented on the 1 km grid-scale:

$$C_{i,t} = \beta_1 P_{i,t} + \beta_2 P_{i,t} D_i + \lambda_i + \gamma_t + \mu_{i,t} \quad (5)$$

where $C_{i,t}$ and $P_{i,t}$ represent productive cropland area and precipitation in grid i in year t, respectively. D_i represents the Euclidean distance from grid i to the nearest urban area with severe NTL reduction. λ_i is an individual fixed effect. γ_t is a time fixed effect. $\mu_{i,t}$ denotes the error term. β_1, β_2 are coefficients that need to be estimated. β_1 represents the impact of precipitation on cropland area, and β_2 denotes how the impact of precipitation varied with D_i, indicating the spatial heterogeneity of precipitation impacts.

Reporting summary. Further information on research design is available in the Nature Research Reporting Summary linked to this article.

Data availability

The data used in this study are available at https://drive.google.com/drive/folders/1Ldkl_kJ9zsFJbn4diP2-FbQSqbQG2EiE?usp=sharing. Annual productive cropland maps (30 m) and NTL maps (1 km) are also available at Zenodo (https://zenodo.org/record/5706374#.YbOY7dDMIuV). Precipitation data are downloadable at: https://chrsdata.eng.uci.edu/. Source data are provided with this paper.

Code availability

The code needed to reproduce the results, figures and tables is fully available at https://github.com/whulixiya/Civil-war-hinders-crop-production-and-threatens-food-security-in-Syria.git.

Received: 31 May 2021; Accepted: 11 November 2021;

References

1. *Emergency Dashboard* (World Food Programme, 2020); https://docs.wfp.org/api/documents/63f55e0cce754924af7819e69d6af68a/download
2. Said, R. & Francis, E. Syrian Kurdish authorities to stop wheat going to government territory. *Reuters* (12 June 2019); https://www.reuters.com/article/uk-syria-wheat-northeast-idUKKCN1TD1KJ
3. *FAO/WFP Crop and Food Security Assessment Mission to the Syrian Arab Republic* (FAO, 2018); http://www.fao.org/3/ca5934en/ca5934en.pdf
4. *More Syrians than Ever Before in the Grip of Hunger and Poverty* (World Food Programme, 2020); https://www.wfp.org/news/more-syrians-ever-grip-hunger-and-poverty
5. Prins, E. Use of low cost Landsat ETM+ to spot burnt villages in Darfur, Sudan. *Int. J. Remote Sens.* **29**, 1207–1214 (2007).
6. Sulik, J. J. & Edwards, S. Feature extraction for Darfur: geospatial applications in the documentation of human rights abuses. *Int. J. Remote Sens.* **31**, 2521–2533 (2010).
7. Witmer, F. D. & O'Loughlin, J. Satellite data methods and application in the evaluation of war outcomes: abandoned agricultural land in Bosnia-Herzegovina after the 1992–1995 conflict. *Ann. Assoc. Am. Geogr.* **99**, 1033–1044 (2009).
8. Nackoney, J. et al. Impacts of civil conflict on primary forest habitat in northern Democratic Republic of the Congo, 1990–2010. *Biol. Conserv.* **170**, 321–328 (2014).
9. Li, X. & Li, D. Can night-time light images play a role in evaluating the Syrian crisis? *Int. J. Remote Sens.* **35**, 6648–6661 (2014).
10. Li, X., Li, D., Xu, H. & Wu, C. Intercalibration between DMSP/OLS and VIIRS night-time light images to evaluate city light dynamics of Syria's major human settlement during Syrian civil war. *Int. J. Remote Sens.* **38**, 5934–5951 (2017).
11. Jiang, W., He, G., Long, T. & Liu, H. Ongoing conflict makes Yemen dark: from the perspective of nighttime light. *Remote Sens.* **9**, 798 (2017).
12. Jaafar, H. H. et al. Impact of the Syrian conflict on irrigated agriculture in the Orontes basin. *Int. J. Water Resour. Dev.* **31**, 436–449 (2015).
13. Jaafar, H. H. & Woertz, E. Agriculture as a funding source of ISIS: a GIS and remote sensing analysis. *Food Policy* **64**, 14–25 (2016).
14. Eklund, L. et al. How conflict affects land use: agricultural activity in areas seized by the Islamic State. *Environ. Res. Lett.* **12**(5), 054004 (2017).
15. Kelley, C. P. et al. Climate change in the Fertile Crescent and implications of the recent Syrian drought. *Proc. Natl Acad. Sci. USA* **112**, 3241–3246 (2015).
16. Brown, O., Hammill, A. & McLeman, R. Climate change as the 'new' security threat: implications for Africa. *Int. Aff.* **83**, 1141–1154 (2007).
17. Barnett, J. & Adger, W. N. Climate change, human security and violent conflict. *Polit. Geogr.* **26**, 639–655 (2007).
18. Ash, K. & Obradovich, N. Climatic stress, internal migration, and Syrian civil war onset. *J. Conflict Resolut.* **64**, 3–31 (2020).
19. Snyder, K. A. & Tartowski, S. L. Multi-scale temporal variation in water availability: implications for vegetation dynamics in arid and semi-arid ecosystems. *J. Arid Environ.* **65**(2), 219–234 (2006).
20. Iizumi, T. & Ramankutty, N. How do weather and climate influence cropping area and intensity? *Glob. Food Sec.* **4**, 46–50 (2015).
21. Bring, J. How to standardize regression coefficients. *Am. Stat.* **48**(3), 209–213 (1994).
22. *Nearly 585,000 People Have Been Killed since the Beginning of the Syrian Revolution* (Syrian Observatory for Human Rights, 2020); https://www.syriahr.com/en/152189
23. *Syria Regional Refugee Response: Inter-agency Information Sharing Portal* (United Nations High Commissioner for Refugees, 2020); https://data2.unhcr.org/en/situations/syria
24. Tull, K. *Agriculture in Syria. K4D Helpdesk Report* (Institute of Development Studies, 2017).
25. *Syria: Shelter Sector 2016 Year-End Report* (Global Shelter Cluster, 2020); https://www.sheltercluster.org/sites/default/files/docs/shelter_sector_2016_year-end_report_final_0.pdf
26. *Syria: 2012 Wheat Production Outlook Is Favorable Despite Ongoing Conflict* (United States Department of Agriculture, 2020); https://ipad.fas.usda.gov/highlights/2012/06/Syria
27. Live Universal Awareness Map Liveuamap. https://syria.liveuamap.com (2020).
28. Mohamed, M. A., Anders, J. & Schneider, C. Monitoring of changes in land use/land cover in Syria from 2010 to 2018 using multitemporal landsat imagery and GIS. *Land* **9**, 226 (2020).
29. *4.3m People in Need of Food Security and Livelihoods Support in Northwest Syria* (United Nations Office for the Coordination of Humanitarian Affairs, 2020); https://reliefweb.int/report/syrian-arab-republic/43m-people-need-food-security-and-livelihoods-support-northwest-syria-23
30. *Syria Dynamic Monitoring Report* (Information Management Unit, 2017); https://www.acu-sy.org/en/wp-content/uploads/2017/04/ACU-IMU-DYNAMO-6-Eng.pdf
31. Christou, W. & Al Nofal, W. Damascus struggles to import food as Syrians go hungry. *Syria Direct* (3 September 2020); https://syriadirect.org/news/damascus-struggles-to-import-food-as-syrians-go-hungry
32. Bishara, Yara and Specia, Megan. 'I dream in fruit': what hunger looks like in Syria. *The New York Times* https://www.nytimes.com/interactive/2016/10/28/world/middleeast/syria-hunger.html (28 October 2016).
33. Harrowell, E. Looking for the future in the rubble of Palmyra: destruction, reconstruction and identity. *Geoforum* **69**, 81–83 (2016).
34. Syrian refugee exodus grows. *Reuters* (10 April 2012) https://www.reuters.com/article/us-syria-refugees/factbox-syrian-refugee-exodus-grows-idUSBRE8390JE20120410
35. *FAO/WFP Crop and Food Security Assessment Mission to the Syrian Arab Republic* (FAO, 2015); http://www.fao.org/3/ca5934en/ca5934en.pdf
36. Andrew, M. L. Weather, wheat, and war: security implications of climate variability for conflict in Syria. *J. Peace Res.* **58**(1), 114–131 (2021).
37. *Timeline: The Rise, Spread, and Fall of the Islamic State* (The Wilson Center Digital Archive, 2019); https://www.wilsoncenter.org/article/timeline-the-rise-spread-and-fall-the-islamic-state
38. Fick, M. Special report: for Islamic State wheat season sows seeds of discontent. *Reuters* (20 January 2015); www.reuters.com/article/us-mideast-crisis-planting-specialreport-idUSKBN0KT0W420150120
39. Song, X. P. et al. Massive soybean expansion in South America since 2000 and implications for conservation. *Nat. Sustain.* **4**, 784–792 (2021).
40. Curtis, E. W. et al. Free access to Landsat imagery. *Science* **320**(5879), 1011–1011 (2008).
41. Michael, A. W. et al. Landsat continuity: issues and opportunities for land cover monitoring. *Remote Sens. Environ.* **112**(3), 955–969 (2008).
42. Masek, J. G. et al. A Landsat surface reflectance dataset for North America, 1990–2000. *IEEE Geosci. Remote Sens. Lett.* **3**(1), 68–72 (2006).
43. Vermote, E., Justice, C., Claverie, M. & Franch, B. Preliminary analysis of the performance of the Landsat 8/OLI land surface reflectance product. *Remote Sens. Environ.* **185**, 46–56 (2016).
44. Zhu, Z. & Woodcock, C. E. Object-based cloud and cloud shadow detection in Landsat imagery. *Remote Sens. Environ.* **118**, 83–94 (2012).
45. Noel, G. et al. Google Earth Engine: planetary-scale geospatial analysis for everyone. *Remote Sens. Environ.* **202**, 18–27 (2017).
46. Didan, K. *MOD13Q1 MODIS/Terra Vegetation Indices 16-Day L3 Global 250m SIN Grid V006 Data Set* (2015); https://doi.org/10.5067/MODIS/MOD13Q1.006
47. Ren, J., Chen, Z., Zhou, Q. & Tang, H. Regional yield estimation for winter wheat with MODIS-NDVI data in Shandong, China. *Int. J. Appl. Earth Obs. Geoinf.* **10**(4), 403–413 (2008).
48. Elvidge, C. D., Baugh, K. E., Zhizhin, M. & Hsu, F. C. Why VIIRS data are superior to DMSP for mapping nighttime lights. *Proc. Asia-Pacific Adv. Netw.* **35**, 62 (2013).

49. Ashouri, H. et al. PERSIANN-CDR: daily precipitation climate data record from multisatellite observations for hydrological and climate studies. *Bull. Am. Meteorol. Soc.* **96**(1), 69–83 (2021).
50. Tucker, C. J. Red and photographic infrared linear combinations for monitoring vegetation. *Remote Sens. Environ.* **8**, 127–150 (1979).
51. Gao, B. C. NDWI-A normalized difference water index for remote sensing of vegetation liquid water from space. *Remote Sens. Environ.* **58**(3), 257–266 (1996).
52. Breiman, L. Random forests. *Mach. Learn* **45**(1), 5–32 (2001).
53. Rodriguez-Galiano, V. F. et al. An assessment of the effectiveness of a random forest classifier for land-cover classification. *ISPRS J. Photogramm. Remote Sens.* **67**, 93–104 (2012).
54. Tom, G. F. et al. The Shuttle Radar Topography Mission. *Rev. Geophys.* **45**(2), RG2004 (2007).
55. Xu, Y. D. et al. Monitoring cropland changes along the Nile River in Egypt over past three decades (1984–2015) using remote sensing. *Int. J. Remote Sens.* **38**(15), 4459–4480 (2017).
56. Olofsson, P. et al. Good practices for estimating area and assessing accuracy of land change. *Remote Sens. Environ.* **148**, 42–57 (2014).
57. Levin, N. et al. Remote sensing of night lights: a review and an outlook for the future. *Remote Sens. Environ.* **237**, 111443 (2020).
58. Li, X. et al. Night-time light dynamics during the iraqi civil war. *Remote Sens.* **10**(6), 858 (2018).
59. Levin, N., Ali, S. & Crandall, D. Utilizing remote sensing and big data to quantify conflict intensity: the Arab Spring as a case study. *Appl. Geogr.* **94**, 1–17 (2018).
60. Pettersson, T. & Oberg, M. Organized violence, 1989–2019. *J. Peace Res.* **57**, 597–613 (2020).
61. *Eight Year Anniversary of the Syrian Civil War: Thematic Assessment of Satellite Identified Damage* (United Nations Office for the Coordination of Humanitarian Affairs, 2021); https://reliefweb.int/sites/reliefweb.int/files/resources/reach_thematic_assessment_syrian_cities_damage_atlas_march_2019_reduced_file_size_1.pdf
62. Mohammed, S. A., Alkerdi, A., Nagy, J. & Harsányi, E. Syrian crisis repercussions on the agricultural sector: case study of wheat, cotton and olives. *Reg. Sci. Pol. Prac.* **12**(3), 519–537 (2020).
63. Tilahun, K. Analysis of rainfall climate and evapo-transpiration in arid and semi-arid regions of Ethiopia using data over the last half a century. *J. Arid Environ.* **64**(3), 474–487 (2006).
64. Müller, M. F. et al. Impact of the Syrian refugee crisis on land use and transboundary freshwater resources. *Proc. Natl Acad. Sci. USA* **113**, 14932–14937 (2016).

Acknowledgements

We acknowledge the High Performance Computing Center at Texas Tech University for providing computational resources that have contributed to the research results reported in this paper. We thank the reviewers and the editor for their constructive comments, which have greatly improved the paper.

Author contributions

X.-P.S. conceived the study and designed cropland mapping and counterfactual analysis. X.L. and D.L. designed the NTL assessment. Z.F. designed the panel regression analysis. X.-Y.L., X.L., Z.F., Z.S. and X.-P.S. conducted the data analysis. All authors contributed to interpretation of the results. X.-Y.L., X.L., M.L. and X.-P.S. wrote the drafts with input from all authors.

Competing interests

The authors declare no competing interests.

Additional information

Supplementary information The online version contains supplementary material available at https://doi.org/10.1038/s43016-021-00432-4.

Correspondence and requests for materials should be addressed to Xi Li or Xiao-Peng Song.

Peer review information *Nature Food* thanks Florian Schierhorn, Sergii Skakun and the other, anonymous, reviewer(s) for their contribution to the peer review of this work.

nature research

Corresponding author(s): Xiao-Peng Song, Xi Li

Last updated by author(s): Nov 5, 2021

Reporting Summary

Nature Research wishes to improve the reproducibility of the work that we publish. This form provides structure for consistency and transparency in reporting. For further information on Nature Research policies, see our Editorial Policies and the Editorial Policy Checklist.

Statistics

For all statistical analyses, confirm that the following items are present in the figure legend, table legend, main text, or Methods section.

n/a	Confirmed	
☐	☒	The exact sample size (*n*) for each experimental group/condition, given as a discrete number and unit of measurement
☐	☒	A statement on whether measurements were taken from distinct samples or whether the same sample was measured repeatedly
☒	☐	The statistical test(s) used AND whether they are one- or two-sided *Only common tests should be described solely by name; describe more complex techniques in the Methods section.*
☒	☐	A description of all covariates tested
☒	☐	A description of any assumptions or corrections, such as tests of normality and adjustment for multiple comparisons
☐	☒	A full description of the statistical parameters including central tendency (e.g. means) or other basic estimates (e.g. regression coefficient) AND variation (e.g. standard deviation) or associated estimates of uncertainty (e.g. confidence intervals)
☒	☐	For null hypothesis testing, the test statistic (e.g. *F*, *t*, *r*) with confidence intervals, effect sizes, degrees of freedom and *P* value noted *Give P values as exact values whenever suitable.*
☒	☐	For Bayesian analysis, information on the choice of priors and Markov chain Monte Carlo settings
☒	☐	For hierarchical and complex designs, identification of the appropriate level for tests and full reporting of outcomes
☒	☐	Estimates of effect sizes (e.g. Cohen's *d*, Pearson's *r*), indicating how they were calculated

Our web collection on statistics for biologists contains articles on many of the points above.

Software and code

Policy information about availability of computer code

Data collection	Google Earth Engine (https://code.earthengine.google.com/) provided the satellite data and climate data (also available at: https://chrsdata.eng.uci.edu/). High-resolution images were visualized within Google Earth.
Data analysis	Google Earth Engine, Matlab (version R2014a), and Python (version 3.7.1) were used to perform image processing as described in the Methods section and Supplementary Information. The custom code is available at https://github.com/whulixiya/Satellite-assessment-of-the-impact-of-Syrian-civil-war-on-extent-of-cultivated-cropland.git. Statistics were mainly performed with IBM SPSS Statistics (version 22.0) and Microsoft Excel 2016. Panel regression analysis was conducted in Eviews (version 8.0). Maps are produced in ArcMap 10.8.

For manuscripts utilizing custom algorithms or software that are central to the research but not yet described in published literature, software must be made available to editors and reviewers. We strongly encourage code deposition in a community repository (e.g. GitHub). See the Nature Research guidelines for submitting code & software for further information.

Data

Policy information about availability of data

All manuscripts must include a data availability statement. This statement should provide the following information, where applicable:

- Accession codes, unique identifiers, or web links for publicly available datasets
- A list of figures that have associated raw data
- A description of any restrictions on data availability

The authors declare that the main data supporting the findings of this study are available in the article and its Supplementary Information files.

The raw data that support the findings of this study are available at https://drive.google.com/drive/folders/1Ldkl_kJ9zsFJbn4diP2-FbQSqbQG2EiE?usp=sharing. Additional data are available from the corresponding authors upon request.

Field-specific reporting

Please select the one below that is the best fit for your research. If you are not sure, read the appropriate sections before making your selection.

☐ Life sciences ☐ Behavioural & social sciences ☒ Ecological, evolutionary & environmental sciences

For a reference copy of the document with all sections, see nature.com/documents/nr-reporting-summary-flat.pdf

Ecological, evolutionary & environmental sciences study design

All studies must disclose on these points even when the disclosure is negative.

Study description	In this study, we evaluated the impact of the Syrian Civil War on cultivated cropland dynamics in Syria from 1998 to 2019 with the combined utility of satellite data and fixed-effects models.
Research sample	Open satellite observations and climate data.
Sampling strategy	A stratified random sample was selected to validate the accuracy of annual cropland maps. 300 pixel locations were selected, and 6,600 pixels were interpreted for the 22 years.
Data collection	Satellite and climate data were collected from Google Earth Engine (https://code.earthengine.google.com/). Night-time light data was downloaded from Yale University (https://urbanization.yale.edu/data) and Colorado School of Mines (https://eogdata.mines.edu/download_dnb_composites.html). Administrative boundary was collected from Version 2.8 of the GADM database of Global Administrative Areas (https://gadm.org/download_country_v2.html). High-resolution images over sample locations were collected from Google Earth.
Timing and spatial scale	Timing scale: 1998-2019 on an annual basis. Spatial scale: at the pixel/grid cell (30m, 1km and 25km), governorate and national scales.
Data exclusions	No data was excluded.
Reproducibility	The numerical results are fully reproducible from the descriptions in the Methods section. All data including the satellite-derived annual cropland maps and night-time light data are shared.
Randomization	Validation sample was randomly selected within each of the three discribed strata.
Blinding	Blinding is not relevant as no experiments were involved.

Did the study involve field work? ☐ Yes ☒ No

Reporting for specific materials, systems and methods

We require information from authors about some types of materials, experimental systems and methods used in many studies. Here, indicate whether each material, system or method listed is relevant to your study. If you are not sure if a list item applies to your research, read the appropriate section before selecting a response.

Materials & experimental systems

n/a	Involved in the study
☒	☐ Antibodies
☒	☐ Eukaryotic cell lines
☒	☐ Palaeontology and archaeology
☒	☐ Animals and other organisms
☒	☐ Human research participants
☒	☐ Clinical data
☒	☐ Dual use research of concern

Methods

n/a	Involved in the study
☒	☐ ChIP-seq
☒	☐ Flow cytometry
☒	☐ MRI-based neuroimaging